Macromolecules

Article

pubs.acs.org/Macromolecules

An Anisotropic Effective Model for the Simulation of Semiflexible Ring Polymers

Peter Poier,*[,†] Christos N. Likos,[†] Angel J. Moreno,[‡,§] and Ronald Blaak[†]

[†]Faculty of Physics, University of Vienna, Boltzmanngasse 5, A-1090 Vienna, Austria

[‡]Centro de Física de Materiales (CSIC-UPV/EHU) and Materials Physics Center (MPC), Paseo Manuel de Lardizabal 5, E-20018 San Sebastián, Spain

[§]Donostia International Physics Center, Paseo Manuel de Lardizabal 4, E-20018 San Sebastián, Spain

ABSTRACT: We derive and introduce anisotropic effective pair potentials to coarse-grain solutions of semiflexible ring polymers of various lengths. The system has been recently investigated by means of full monomer-resolved computer simulations, revealing a host of unusual features and structure formation, which, however, cannot be captured by a rotationally averaged effective pair potential between the rings' centers of mass [Bernabei, M.; et al. *Soft Matter* **2013**, *9*, 1287]. Our new coarse-graining strategy is to picture each ring as a soft, penetrable disk. We demonstrate that for the short- and intermediate-length rings the new model is quite capable of capturing the physics in a quantitative fashion, whereas for the largest rings, which resemble flexible ones, it fails at high densities. Our work opens the way for the physical justification of general, anisotropic penetrable interaction potentials.

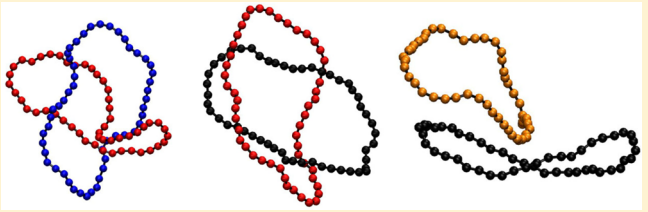

1. INTRODUCTION

By the simple process of joining the ends of a linear polymer chain, one obtains a ring polymer (RP).[1] While the architecture of ring polymers is very simple, they differ in many interesting ways from their linear counterparts and are the subject of active research in physics, biology, chemistry, and even pure mathematics. One interesting consequence is that for a dynamics that disallows strand crossing, there are different classes of configurations of a RP, which can never transform into each other. These are referred to as the *topology classes* or *knot types* of a RP. Knot theory is a fascinating and active branch of mathematics with many open problems concerning the enumeration and classification of knots.[2] A RP that has the topology of a circle is called an *unknotted* RP.

Unlike RPs, linear polymer chains can strictly speaking never be knotted, as every configuration of a linear polymer chain can be continuously transformed to a straight line, without the need for strand crossings. While this is a fundamental difference between linear polymer chains and RPs, it is nevertheless possible to extend the concept of knots to *physical* knots on linear polymer chains.[3] There are many works dealing with the properties of these *physical* knots on linear polymer chains,[4−11] in particular due to their relevance in biophysics, where they are for instance found in DNA[12,13] and can have significant effects on key processes.[14−16]

The topological constraint of a ring polymer has important consequences for its physical behavior. It took the work of many authors[17−24] to establish that the diameter of gyration D_g of an isolated ideal RP with fixed topology scales as $\langle D_g^2 \rangle \sim N^{2\nu}$, where $\nu \approx 0.588$ is the Flory exponent, which also describes the scaling behavior of the radius of gyration of self-avoiding linear chains.[25] This is true for all knot types, even for an ideal unknotted RP (i.e., without monomer excluded volume interactions, just keeping the topological constraints). An ideal linear polymer chain, on the other hand, remains more compact and exhibits the scaling law of a nonself-avoiding random walk $\langle D_g^2 \rangle \sim N$. Another important difference lies in the effective potential between the centers of mass of RPs. While the effective potential vanishes between infinitely thin linear polymer chains and also between an infinitely thin linear polymer chain and a RP, there remains a nonzero repulsive contribution between cyclic polymers with fixed topology.[26,27] Here one usually speaks of a topological potential. Furthermore, it was shown that the effective potential between two moderately sized RPs increases with the knot complexity of the rings.[27]

Also for concentrated systems, the topology of polymer chains plays an important role. The scaling of linear polymer chains in the melt is the one of a nonself-avoiding random walk $\langle D_g^2 \rangle \sim N$. Simulations of dense systems of RPs,[28,29] on the other hand, showed that while short chains also exhibit a Gaussian scaling behavior $\langle D_g^2 \rangle \sim N$, long chains are compact and thus scale as $\langle D_g^2 \rangle \sim N^{2/3}$. In between there is a broad crossover region, where a $\langle D_g^2 \rangle \sim N^{4/5}$ scaling provides a good description of the data. For the dynamics, it is expected that concatenations of ring polymers can have a significant effect, as they are permanent, in contrast to the entanglement of linear polymer chains. However, this implies that those concate-

Received: March 23, 2015
Revised: May 29, 2015
Published: July 10, 2015

DOI: 10.1021/acs.macromol.5b00603
Macromolecules 2015, 48, 4983−4997

nations are there in the first place, i.e., from the very synthesis of the sample on. Even in the absence of concatenations, there are important differences in the dynamics of RPs in the melt with respect to their linear counterparts. For instance, recent experiments[30] and simulations[31] revealed a power-law stress relaxation instead of the rubbery plateau found for linear chains.

For the large intermediate density domain between dilute solutions and melts, there are relatively few theoretical results despite the practical relevance of this regime for instance in the field of biophysics, where the topological interactions between chromatin loops plays a crucial role in the creation of chromosome territories.[26,32−34] A fruitful and modern approach for the economic description and simulation of macromolecules in this regime is the method of coarse-graining. The idea behind this method is to bridge the time and length scales in the system by describing the macromolecules via an effective model with a reduced set of suitably chosen effective degrees of freedom (dof). The microscopic information on the monomer-resolved model is underlying the effective model, as it determines the form of the effective potential, which describes the interaction between the macromolecules. The advantage of this method is not only that every time step in a simulation requires less computational effort due to the simplified representation but also that one can often choose a much larger time step in a simulation of the coarse grained model, as the dof that remain in the coarse-grained model change much slower in time than their counterparts in the monomer-resolved model.[35,36]

The method of coarse-graining is well-established and has for instance found successful application for polymer chains,[37−39] star polymers,[40−43] star-shaped polyelectrolytes,[44,45] dendrimers,[46−48] and block copolymers.[49−51] The identification of the relevant degrees of freedom is an essential part in the design of an effective model. One often uses isotropic effective models, where the macromolecules consisting of many individual monomers are reduced to their center of mass. For the semiflexible ring polymers such a model has already been investigated in ref 52. Clustering was observed in monomer-resolved simulations of semiflexible ring polymers as well as in the corresponding isotropic effective model. However, it was also shown that the monomer-resolved system shows anisotropic features that cannot be accounted for in the isotropic effective model. Also, the correlation functions stemming from the isotropic effective model are markedly different from the microscopically derived ones. Anisotropy is particularly strong for rings with high bending stiffness or few monomers, as they have a strong tendency to orient with respect to other rings in their proximity. This motivates us to introduce an anisotropic effective model for the description of semiflexible ring polymers in this article. In this model, we will define the effective particles as soft disk-like molecules which are described not only by their center of mass but also by the direction in which their faces are oriented. An anisotropic effective model was already used successfully for the description of hard disk-like macromolecules,[53] but to the best of our knowledge this approach was up to now never applied to penetrable macromolecules, where the centers of mass of the macroparticles can coincide. Penetrable particles are particularly interesting as they allow for clustering, which often leads to a rich phase behavior. For instance, point-particles interacting with a certain class of ultrasoft potentials form so-called cluster crystals.[54−56] Unlike in an ordinary crystal multiple soft particles can sit on top of each other at the same lattice site in a cluster crystal. Another peculiar feature of this state of matter is that by compressing it one only changes the occupation number of particles per lattice site, while the lattice constant remains invariant. Monomer-resolved simulations of semiflexible ring polymers, on the other hand, show the formation of the cluster glass phase,[57,58] which is an arrested state that also contains some of the features found in the cluster crystal phase. In both cases the overall structure of the system is frozen, while individual particles can hop between the lattice sites of the cluster crystal or the stacks found in the cluster glass. Elongated dendrimers, which unlike hard rod-like particles exhibit local antinematic order,[59] are another interesting example for a system of penetrable particles, which behaves distinctively different to its solid counterpart. By creating an anisotropic effective model for the semiflexible ring polymers, we aim at a model that is still computationally cheap and that improves the description obtained by the isotropic model, especially for the case of high densities. In addition, the analysis of the interactions in the anisotropic effective potential allows us to get a better understanding for the interaction between the anisotropic, penetrable nanoparticles in systems of semiflexible RPs.

The remainder of this article is structured as follows. In section 2 we first present the Hamiltonian of the monomer-resolved model which we use for the description of semiflexible RPs and then introduce an anisotropic effective model for such a system. In section A of the Appendix we give more details about the derivation of the effective interactions for such a model. We carried out molecular dynamics simulations of the monomer-resolved model and Monte Carlo simulations of the effective models; details concerning these simulations are given in section 3. In section 4 we present the anisotropic effective potential and discuss its features. Results of Monte Carlo simulations with this potential, which show that the inclusion of anisotropy in the effective model can significantly improve the agreement with the monomer-resolved model, are presented in section 5, whereas in section 6 we briefly discuss the effects of truncation of the expansion of the potential on the quality of the results. Conclusions are given in section 7. In the Appendix, we explain the expansion of the anisotropic pair-correlation function of a system of two RPs, which contains all the information for calculating the effective potential, as a sum of suitably chosen basis functions.

2. ANISOTROPIC EFFECTIVE MODEL

2.1. Monomer-Resolved Model for Semiflexible Ring Polymers. The derivation of the anisotropic effective model is based on a microscopic model of semiflexible ring polymers, each consisting of N monomers. They are described with the bead−spring model by Kremer and Grest[60] and an additional rigidity term. Thus, any two monomers interact via the truncated and shifted Lennard-Jones potential

$$V_{\mathrm{LJ}}(r) = \begin{cases} 4\epsilon\left[\left(\frac{\sigma}{r}\right)^{12} - \left(\frac{\sigma}{r}\right)^{6} + \frac{1}{4}\right] & \text{if } r < 2^{1/6}\sigma \\ 0 & \text{if } r \geq 2^{1/6}\sigma \end{cases} \quad (1)$$

This potential is purely repulsive, accounting then for monomer excluded volume interactions. Bonded monomers also interact through a finitely extensible nonlinear elastic potential (FENE)

DOI: 10.1021/acs.macromol.5b00603
Macromolecules 2015, 48, 4983−4997

$$V_{\mathrm{FENE}}(r) = -\frac{kR_0^{\,2}}{2}\ln\left[1 - \left(\frac{r}{R_0}\right)^2\right] \tag{2}$$

Rigidity is introduced via the bending potential

$$V_{\mathrm{bend}}(\theta) = \kappa(1 - \cos\theta)^2 \tag{3}$$

where θ is the angle between two consecutive bond vectors. [Note that this is not the Kratky–Porod model (linear in the cosine). We expect the same qualitative results for Kratky–Porod rings with the same N's and persistence lengths as the model simulated here.] The potential V_{bend} vanishes for $\theta = 0$, when the polymer chain does not bend at the respective angle. We choose $\epsilon = k_{\mathrm{B}}T$, $k = 30k_{\mathrm{B}}T/\sigma^2$, $R_0 = 1.5\sigma$, and $\kappa = 30k_{\mathrm{B}}T$, where k_{B} is the Boltzmann constant and T the temperature. These are precisely the parameters employed in the simulation study of ref 52. The corresponding dynamics does not allow for chain crossings and thus topology is preserved.

In ref 58 the characteristic ratio[61] of this polymer model was estimated by carrying out simulations of isolated linear chains. Excluded volume interactions were switched off except for mutually connected monomers in order to obtain long-range Gaussian statistics. C_∞ was obtained by analyzing the long-s limit of the ratio $\langle R^2(s)\rangle/s\langle b^2\rangle$, where $R(s)$ is the distance between two monomers i, j with $s = |i - j|$, and b is the bond length ($\langle b^2\rangle = 0.94$). The authors reported a value of $C_\infty \sim 15$, which is typical for stiff polymers.[61] We can give an estimate for the persistence length of the model by mapping it to the freely rotating chain model using the relation $\cos\theta = (C_\infty - 1)/(C_\infty + 1)$, where θ is the bending angle of the freely rotating chain model.[61] The persistence length is then obtained as $s_p b = -b/\ln(\cos\theta) \sim 7.3$. We carried out simulations of ring polymers with $N = 20$, 50, and 100 monomers, which have the contour to persistence length ratio $N/s_p \sim 2.7$, 6.7, and 13.3, respectively.

2.2. Anisotropic Effective Model. In earlier work,[52] Bernabei et al. carried out extensive monomer-resolved simulations of stiff ring polymers to obtain the structure of concentrated solutions of the same. In an attempt to coarse-grain the system in the simplest possible way, they also derived and employed an isotropic effective potential for their effective description, reducing thereby stiff RP's into point-like effective particles, namely their centers of mass. At this level of approximation, the effective particles possess no other internal (spin-like) degrees of freedom, and thus the effective interaction is isotropic. The effective potential between these macroparticles was defined by calculating the pair correlation function $g^{\mathrm{iso}}(r)$ in an infinitely dilute system and using

$$\beta V_{\mathrm{eff}}^{\mathrm{iso}}(r) \equiv -\ln[g^{\mathrm{iso}}(r)] \tag{4}$$

to define the effective interaction potential between these point particles, where $\beta = 1/(k_{\mathrm{B}}T)$. In the infinitely dilute case, the distribution of the centers of mass of the ring polymers in equilibrium is identical to the distribution of the point particles in the effective model. At higher densities, however, it turns out that multiparticle terms in the effective potential are necessary to obtain the correct equilibrium distribution of the centers of mass in the effective model. One of the reasons due to which multiparticle interactions become important is that two ring polymers that are sufficiently close and stiff will prefer to align parallel to each other. A third ring polymer interacting with those two will not see them as two independent rings but as a system of two rings that are correlated. When using the potential $V_{\mathrm{eff}}(r)$ calculated in eq 4, one assumes that the free energy penalty of one ring with respect to a second is independent of the presence of another polymer in the vicinity of the second. If the ring polymers preferentially align parallel, this assumption is clearly violated and one has to correct the effective potential by introducing multiparticle terms. Bernabei et al. showed that already at moderate densities one can encounter strong correlations of the orientations of the semiflexible ring polymers, in particular if the chains contain only few monomers (e.g., $N = 20$).[52] Therefore, a more accurate coarse-graining which takes into account the ring anisotropy is called for.

The easiest way to incorporate the correlations of the orientations of rings is to introduce them via additional degrees of freedom (dof) in the effective description. This is precisely what we do in this article. For this purpose, we need to first come up with a suitable definition for the orientation of a RP. To this end, we make use of the gyration tensor

$$S_{\alpha\beta} = \frac{1}{N}\sum_{i=1}^{N} r_\alpha^{(i)} r_\beta^{(i)} \tag{5}$$

where $r_\alpha^{(i)}$ ($\alpha = x, y, z$, Cartesian components) denotes the position of the ith monomer with respect to the center of mass of the ring to which this monomer belongs. The eigenvectors of $S_{\alpha\beta}$ are the principal axes of an ellipsoid that approximates the shape of the macromolecule: If a RP is flat, which means that all its monomers lie in one plane, the ellipsoid has one zero eigenvalue with a corresponding eigenvector that is perpendicular to that plane. Also in the more general case, where the monomers do not all lie in the same plane, we define the normalized eigenvector corresponding to the smallest eigenvalue of $S_{\alpha\beta}$ as the direction vector $\mathbf{d}$ of the RP. Note that $\mathbf{d}$ and $-\mathbf{d}$ are equivalent for reasons of symmetry. The ring polymers in the anisotropic effective model we propose are described via the position vectors of their centers of mass, $\mathbf{R}^{(i)}$, and their direction vector, $\mathbf{d}^{(i)}$. Henceforth, we describe the stiff rings as soft circular disks and ignore differences in the other two eigenvectors of the gyration tensor $S_{\alpha\beta}$. This choice is motivated by the limit of infinite bending stiffness, where the rings assume flat and precisely circular conformations. Our model therefore amounts to the *minimal* anisotropic extension of the spherically symmetric effective interaction between the centers of mass. We emphasize, however, that there is no *a priori* guarantee that this will be an improvement over the isotropic model at finite densities and in particular at high concentrations: this depends on the degree in which the RP's at high concentration maintain their anisotropic shape and properties encoded in the high-dilution limit in which the anisotropic pair potential is derived. Accordingly, the introduction of such a potential is not a straightforward part of a systematic strategy of introducing more and more detail into the effective description of the system.

In order to determine the anisotropic effective potential V_{eff}, we carried out monomer-resolved simulations of two ring polymers inside a large simulation box. The effective pair potential is then defined such that it exactly reproduces the correlation functions of the effective degrees of freedom in this infinitely dilute, monomer-resolved simulation. In the effective model, two ring polymers are described by a total of 10 degrees of freedom—three for each center of mass and two for each direction vector of each ring polymer. However, due to translation, rotation, and mirror symmetry, the distinct configurations (those that cannot be related by symmetry

DOI: 10.1021/acs.macromol.5b00603
Macromolecules 2015, 48, 4983–4997

transformations) of a system with two effective particles are reduced and can be specified by four parameters only.

A convenient choice for these variables is illustrated in Figure 1 and reads as follows:

$$r \equiv |\mathbf{r}|$$
$$\cos\theta_1 \equiv \mathbf{d}^{(1)}\cdot\hat{\mathbf{r}}$$
$$\cos\theta_2 \equiv \mathbf{d}^{(2)}\cdot\hat{\mathbf{r}}$$
$$\varphi \equiv \arccos\left(\frac{\mathbf{d}_\perp^{(1)}\cdot\mathbf{d}_\perp^{(2)}}{|\mathbf{d}_\perp^{(1)}||\mathbf{d}_\perp^{(2)}|}\right) \quad (6)$$

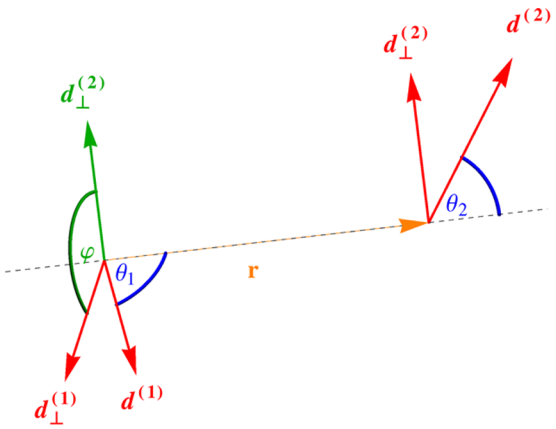

Figure 1. Illustration of the effective variables $r = |\mathbf{r}|$, θ_i, and φ with which relative configurations of ring polymers are described.

where $\mathbf{r} \equiv \mathbf{R}^{(2)} - \mathbf{R}^{(1)}$ is the connection vector between the centers of mass of the two rings, $\hat{\mathbf{r}} \equiv \mathbf{r}/r$ the unit vector in the direction of $\mathbf{r}$, and $\mathbf{d}_\perp^{(i)}$ the component of the director $\mathbf{d}^{(i)}$ perpendicular to $\mathbf{r}$; $0 \le \varphi \le \pi$ denotes the angle between vectors $\mathbf{d}_\perp^{(1)}$ and $\mathbf{d}_\perp^{(2)}$. By selecting the appropriate sign of $\mathbf{d}^{(i)}$, we can always choose $\cos\theta_i$ to lie in the interval $[0, 1]$.

Let us define the ideal case as the system where the effective particles do not interact, and thus every orientation and position of the effective particles occur with equal probability, independently of the configuration of the other effective particle. With the effective coordinates defined in eq 6 the probability density in the ideal system, $P_{\mathrm{id}}(r, \cos\theta_1, \cos\theta_2, \varphi)$ is proportional to r^2 and constant in both $\cos\theta_i$ and φ. This simple behavior of $P_{\mathrm{id}}(r, \cos\theta_1, \cos\theta_2, \varphi)$, makes eq 6 a particularly convenient choice of the effective coordinates. In the simulations with two ring polymers, we obtain a probability density $P(r, \cos\theta_1, \cos\theta_2, \varphi)$ that is different from the ideal distribution P_{id}. We define as a generalized version of the radial distribution function the anisotropic pair correlation function as

$$g(r, \cos\theta_1, \cos\theta_2, \varphi) = \frac{P(r, \cos\theta_1, \cos\theta_2, \varphi)}{P_{\mathrm{id}}(r, \cos\theta_1, \cos\theta_2, \varphi)} \quad (7)$$

Thus, the quantity $g(r, \cos\theta_1, \cos\theta_2, \varphi)$ describes the factor by which configurations in the effective anisotropic model have to be enhanced or suppressed with respect to the ideal case, in order to obtain a distribution for the effective dof that is identical to the distribution obtained in a monomer-resolved simulation in the infinitely dilute case. As in the isotropic case (4) the relation to the associated effective potential reads

$$\beta V_{\mathrm{eff}}(r, \cos\theta_1, \cos\theta_2, \varphi) = -\ln[g(r, \cos\theta_1, \cos\theta_2, \varphi)] \quad (8)$$

From the anisotropic effective potential, we can deduce the isotropic pair-correlation function via

$$g^{\mathrm{iso}}(r) = \frac{1}{\pi}\int_0^1 \mathrm{d}\cos\theta_1 \int_0^1 \mathrm{d}\cos\theta_2 \int_0^\pi \mathrm{d}\varphi\; g(r, \cos\theta_1, \cos\theta_2, \varphi) \quad (9)$$

The associated isotropic effective potential is then given by (4).

The effective potential between two identical ring polymers remains invariant if we swap the orientations of their respective director with respect to the connection vector, i.e., if we swap the values of the polar angles θ_1 and θ_2 of the two rings:

$$V_{\mathrm{eff}}(r, \cos\theta_1, \cos\theta_2, \varphi) = V_{\mathrm{eff}}(r, \cos\theta_2, \cos\theta_1, \varphi) \quad (10)$$

This symmetry is violated for the effective potential between bidisperse ring polymers, e.g., for ring polymers with a different number of monomers. However, apart from this symmetry, there would be no differences in the procedure of calculating the effective potential between different types of ring polymers.

3. SIMULATION DETAILS

3.1. Derivation of the Effective Interaction. To determine the effective potential, we carry out constant *NVT* molecular dynamics simulations with two ring polymers. We simulate rings of N = 20, 50, and 100 monomers. For these simulations we use the LAMMPS simulation package.[62] The polymer rings are placed in a simulation box, which is large enough to prevent multiple interactions via the periodic boundary conditions. The temperature in the simulation is maintained by the use of Langevin dynamics. The corresponding equations of motion read as[63]

$$m\ddot{\mathbf{r}}_i(t) = \mathbf{F}_i(t) - \gamma m\dot{\mathbf{r}}_i(t) + \boldsymbol{\eta}_i(t) \quad (11)$$

Here, $\mathbf{r}_i$ is the position of the ith monomer, m its mass, and $\mathbf{F}_i(t)$ is the deterministic force acting on it, which includes the microscopic forces originating from potentials (1)−(3) and the force originating from a biasing potential. The bias potential $V_{\mathrm{bias}} = (r - r_j)^2 k_j/2$ introduces a harmonic spring with spring constant k_j between the centers of mass of the ring polymers. The spring is relaxed for $r = r_j$. We carried out simulations for different values of r_j, starting at $r_j = 0$ and increasing it up to some maximum value r_c in steps of $\sigma/2$. For N = 20, 50, and 100, r_c was chosen as 10σ, 20σ, and 30σ, respectively. These values for r_c are much bigger than the infinite-dilution diameters of gyration ($D_{g0} = 5.9\sigma$, 13σ, and 21.5σ for N = 20, 50, and 100, respectively). For k_j we chose the values $2.5\epsilon/\sigma^2$ and ϵ/σ^2 for all ring sizes, and for N = 20 we also carried out simulations with $k_j = 5\epsilon/\sigma^2$. The quantity $\boldsymbol{\eta}_i(t)$ is a random force, with $\langle\boldsymbol{\eta}_i(t)\rangle = 0$, which is related to the friction coefficient γ by the fluctuation dissipation relation $\langle\eta_i^\alpha(t)\eta_j^\beta(t')\rangle = 2\gamma m k_B T\delta_{ij}\delta_{\alpha\beta}\delta(t - t')$, α and β denoting Cartesian components. Our unit of time is set by $t_0 = (m\sigma^2/\epsilon)^{1/2}$, and the friction coefficient γ is chosen as $1/t_0$. We integrate the equations of motion with a time step of $\Delta t = 10^{-3}t_0$ and use 2×10^8 timesteps for equilibrating the system and collect data during another 2×10^9 timesteps.

We sample histograms $P^{(j)}(Q)$, where Q refers to a bin in the 4D space of the effective coordinates. $P^{(j)}(Q)$ gives the probability for a state in the jth simulation to have effective coordinates in bin Q. The histograms have 128 bins in r and 16 bins in $\cos\theta_1$, $\cos\theta_2$, and φ direction. As discussed in section A of the Appendix, we use the self-consistent histogram method

DOI: 10.1021/acs.macromol.5b00603
Macromolecules 2015, 48, 4983−4997

by Ferrenberg and Swendsen[64,65] to combine the $P^{(j)}(Q)$ histograms for simulations with identical ring sizes but different biasing potentials to arrive at an estimate for $P(Q)$ in the unbiased system.

3.2. Many-Body Effective Fluid. Using the anisotropic effective potential, we carry out standard metropolis Monte Carlo (MC) simulations for the anisotropic effective model. The values of the anisotropic effective potential have been calculated on a discrete grid in the $(r, \cos\theta_1, \cos\theta_2, \varphi)$ space, and we use linear interpolation to estimate the values of $\exp(-\beta V_{\text{eff}})$ in between the grid points. Having in mind a comparison with both the monomer-resolved simulation results and the isotropic effective potential of ref 52, we choose the same number of particles and effective densities that were used in those simulations. For rings with N = 20, 50, and 100 monomers we simulate systems of n = 2400, 1600, and 1200 rings, respectively, varying in each case accordingly the cubic box size L as to achieve the desired density $\rho = n/L^3$. As the effective potential V_{eff} is bounded, a random distribution of the particles in the simulation box can be used as initial condition. We have implemented two types of MC moves: the first one translates a randomly chosen particle in a random direction, and the second randomly rotates the particle's director by some angle. The distance by which the particles are displaced and the angle by which they are rotated is randomly selected in an interval starting at 0 and going up to some maximum value. For both moves, this maximum value of the interval is chosen such that the acceptance ratio is approximately 15%. We use 9×10^6 MC moves to equilibrate the system. During this equilibration period the individual soft particles diffuse to several times their own diameter. Afterward, during 15×10^6 MC moves equilibrium configurations are generated. We store the configurations every 20×10^3 moves and use them to compute the physical observables that are presented in section 5.

The gain in computational efficiency for the simulations in going from a monomer-resolved to a coarse-grained simulation is considerable. The relevant quantity to consider here would be the velocity through phase space. This can conveniently be characterized by means of the mean-square displacement of the rings per unit of CPU time. If one ignores the detailed implementation aspects, the CPU time spent on a single sweep over all monomers in the former and a run over all effective ring particles in the latter, which strictly speaking depend on both the number of monomers N per ring and the overall density of rings, are of similar magnitude. However, the diffusion per sweep in the coarse-grained simulation is significantly larger than that for the monomer resolved simulation; i.e., for the case of N = 50 and ρ^* = 20 this results in a factor of approximately 10^4. The reason for this dramatic improvement is twofold. First of all, the translation/rotation of an effective ring corresponds to a much more time-consuming collective movement of the constituents. The second even more important contribution arises from the steric interaction that are present in the monomer resolved simulations and prevent the unphysical crossing of chain segments. In the coarse-grained simulations such a restriction is absent; i.e., the effective rings are penetrable and can move apparently through each other. On this level of description this effect is not an unphysical process but should be interpreted as a shortcut connecting initial and final configurations that are connected by a much more time-consuming and physically realizable pathway of folding and collective monomer movements.

4. ANISOTROPIC EFFECTIVE POTENTIAL

We commence by recalculating the *isotropic*, i.e., angularly average, effective pair potential $V_{\text{eff}}^{\text{iso}}(r)$ between the stiff rings as a way of comparison with the previously derived results in ref 52. Results are summarized in Figure 2, reproducing indeed the

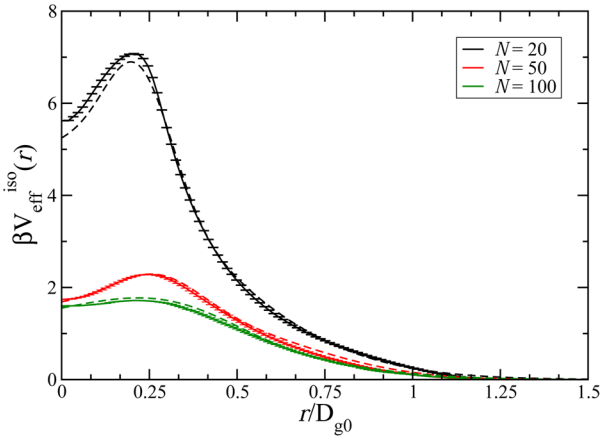

Figure 2. Effective center-of-mass pair potential in the isotropic effective model for rings with different numbers of monomers N. The center-of-mass separation r is scaled with D_{g0}, the average diameter of gyration of a free ring polymer. The solid line shows the angularly averaged effective pair potential, while the dashed lines are results of ref 52.

previously derived ones.[52] The potential for $r = 0$ is finite, as the rings are allowed to overlap. It also features a local minimum there, whereas its maximum is located at $r \approx 0.25D_{g0}$ for all ring types investigated. Here, D_{g0} is the average diameter of gyration of a free ring polymer. The height of the potential barrier at small distances of r decreases by increasing the number of monomers N on the ring polymers.

Going over to the anisotropic effective model, we proceed with computing the aforementioned pair correlation function $g(r, \cos\theta_1, \cos\theta_2, \varphi)$ for a system of two ring polymers. As the latter depends on four effective coordinates and is therefore difficult to visualize, we first introduce a reduced pair correlation function $G(r, \mathbf{d}^{(1)}\cdot\mathbf{d}^{(2)})$, which expresses the relative joint probability density of observing the two ring polymers at a distance r and with the directors mutually oriented at the value given by their scalar product, $\mathbf{d}^{(1)}\cdot\mathbf{d}^{(2)}$, over the same quantity for noninteractive rings. Moreover, we introduce a reduced version of this function, $G(r, \mathbf{d}^{(1)}\cdot\mathbf{d}^{(2)})$, by dividing over its isotropic counterpart, i.e.

$$G(r, \mathbf{d}^{(1)}\mathbf{d}^{(2)}) = \frac{g(r, \mathbf{d}^{(1)}\mathbf{d}^{(2)})}{g^{\text{iso}}(r)} \tag{12}$$

Results are summarized in Figure 3. One can see that the angular distribution of the directors changes significantly for $r \approx 0.25D_{g0}$, which is approximately the position of the maximum of $V_{\text{eff}}^{\text{iso}}(r)$. For $r < 0.25D_{g0}$ the angle between the directors is biased toward $\pi/2$, while for $0.25D_{g0} < r < D_{g0}$ they prefer to align parallel with respect to each other. The position of the maximum of $V_{\text{eff}}^{\text{iso}}(r)$ coincides approximately with the distance r where interpenetrated configurations of the rings become subdominant and where they are more likely to align parallel to each other. The transition between these two domains is particularly steep for N = 20 and becomes smoother for rings with a larger number of monomers. When the rings

DOI: 10.1021/acs.macromol.5b00603
Macromolecules 2015, 48, 4983−4997

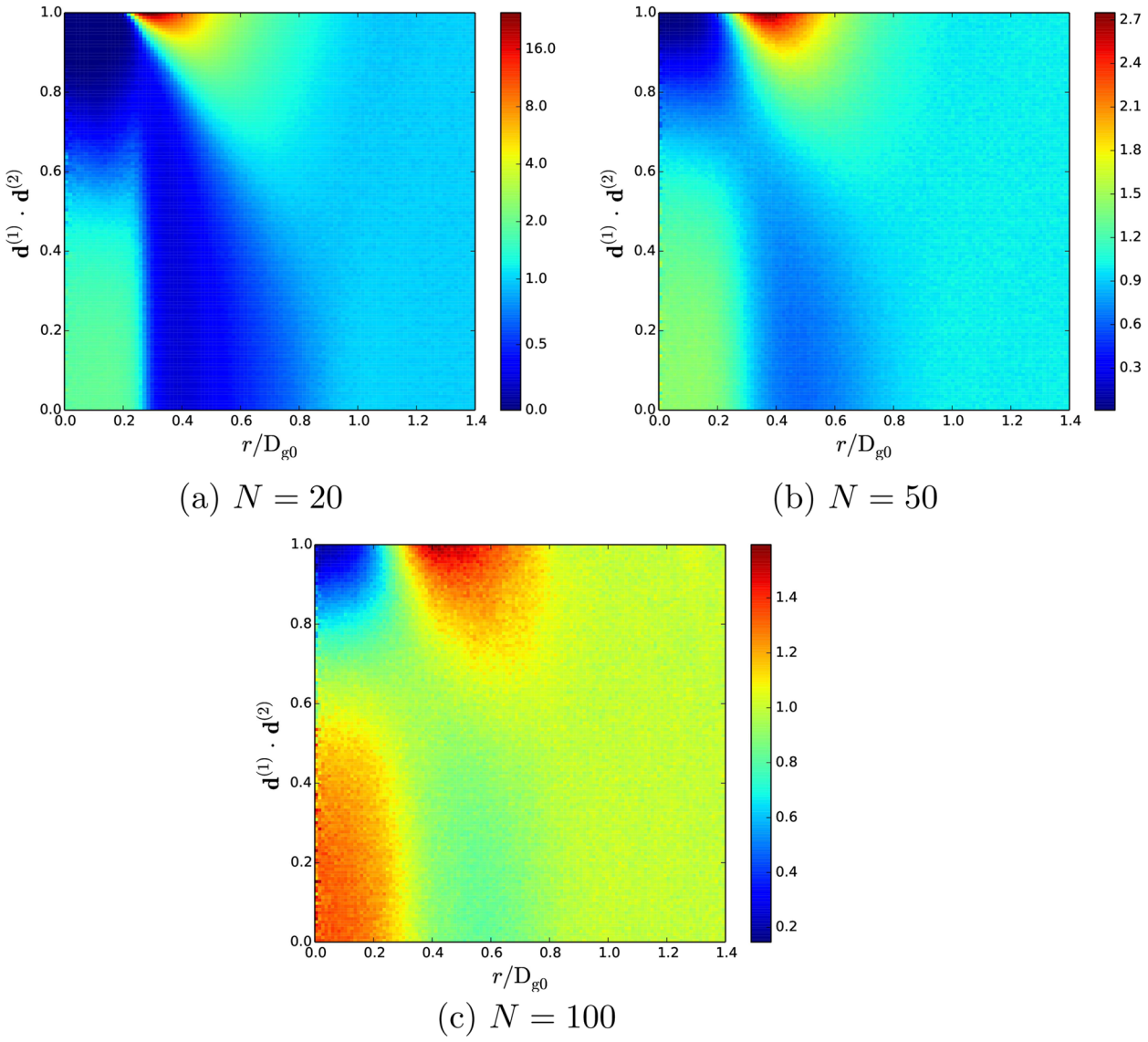

Figure 3. Infinite-dilution limit of the quantity $G(r, \mathbf{d}^{(1)}\cdot\mathbf{d}^{(2)})$, which quantifies the distribution of the scalar product between directors for different values of r. We visualize this distribution for the ring sizes $N = 20$, $N = 50$, and $N = 100$.

interpenetrate each other, the distribution of angles between the directors is rather wide, while it gets narrow after the transition where the bias toward parallel alignments of the rings is very strong in particular for the smallest rings with $N = 20$. It is readily visible from Figure 3 that anisotropy is particularly important for smaller rings. For $r > D_{g0}$, the distribution of the angle between the directors becomes flat, as the rings are then well separated and hence do not interact. Note that by definition, eq 12, the quantity $G(r, \mathbf{d}^{(1)}\cdot\mathbf{d}^{(2)})$, is a normalized probability distribution for *fixed* r, and in Figure 3 it is therefore meaningless to compare the plotted function at different r values.

The relative orientation between the vectors $\mathbf{r}$, $\mathbf{d}^{(1)}$, and $\mathbf{d}^{(2)}$ is of course not completely determined by the scalar product $\mathbf{d}^{(1)}\cdot\mathbf{d}^{(2)}$; the function $G(r, \mathbf{d}^{(1)}\cdot\mathbf{d}^{(2)})$ contains less information than the full correlation function $g(r, \cos\theta_1, \cos\theta_2, \varphi)$. In particular, when the directors are parallel, i.e., $\mathbf{d}^{(1)}\cdot\mathbf{d}^{(2)} = 1$, the angle between the connection vector $\mathbf{r}$ and the directors $\mathbf{d}^{(1)}$ and $\mathbf{d}^{(2)}$ is still arbitrary. We denote a configuration with $\mathbf{d}^{(1)}\|\mathbf{d}^{(2)}\|\mathbf{r}$ as $\rightarrow\rightarrow$ and a configuration with $\mathbf{d}^{(1)}\|\mathbf{d}^{(2)}\perp\mathbf{r}$ as $\uparrow\uparrow$. From the reduced pair correlation function $G(r, \mathbf{d}^{(1)}\cdot\mathbf{d}^{(2)})$ alone, we cannot say which of these two configurations is more probable, as the scalar product $\mathbf{d}^{(1)}\cdot\mathbf{d}^{(2)}$ is identical to 1 in both cases. Using the full anisotropic pair correlation function $g(r, \cos\theta_1, \cos\theta_2, \varphi)$, we can compare the corresponding effective potentials:

$$\beta V_{\rightarrow\rightarrow}(r) = -\ln[g(r,\ \cos\theta_1 = 1,\ \cos\theta_2 = 1,\ \varphi)]$$
$$\beta V_{\uparrow\uparrow}(r) = -\ln[g(r,\ \cos\theta_1 = 0,\ \cos\theta_2 = 0,\ \varphi = 0)] \quad (13)$$

For the $\rightarrow\rightarrow$ case the value of the φ coordinate is immaterial. However, due to the finite bin size of the grid on which we have calculated $g(r, \cos\theta_1, \cos\theta_2, \varphi)$, the choice of φ makes a small difference, even for $V_{\rightarrow\rightarrow}(r)$. We compute $V_{\rightarrow\rightarrow}(r)$ from the average of $g(r, \cos\theta_1 = 1, \cos\theta_2 = 1, \varphi)$ in φ.

In Figure 4 we see that $V_{\uparrow\uparrow}(r)$ increases significantly when r approaches D_{g0}, while $V_{\rightarrow\rightarrow}$ stays close to 0 until much smaller distances r. We can understand this results if we imagine the rings as disks with diameter D_{g0}. In the $\uparrow\uparrow$ configuration, the rings lie in the same plane and will therefore start to overlap as soon as $r \leq D_{g0}$. Since the rings are not perfect circles and their

DOI: 10.1021/acs.macromol.5b00603
Macromolecules 2015, 48, 4983−4997

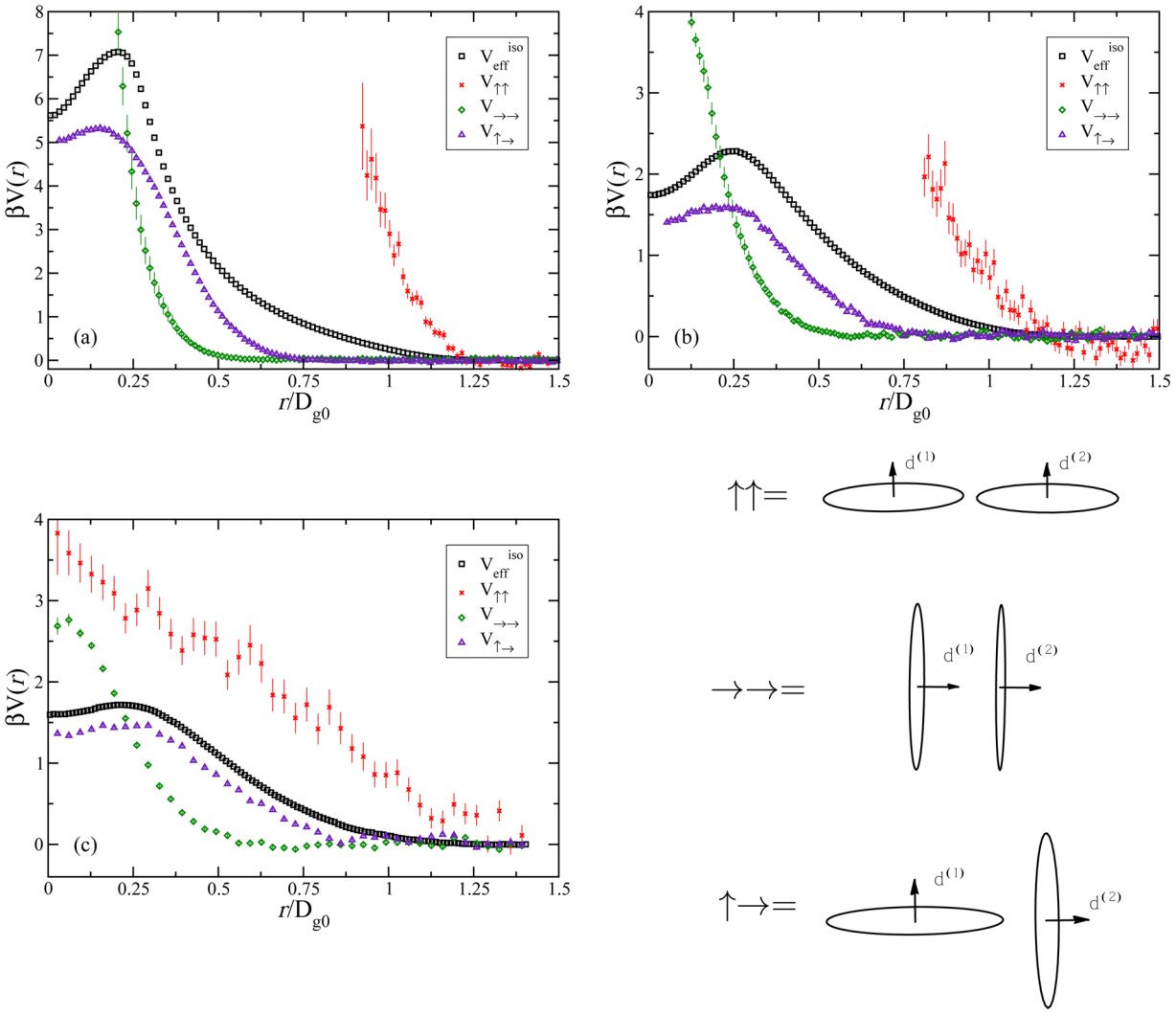

Figure 4. Effective potential for three different fixed configurations of the directors and the connecting vector. As a comparison, we also plot the pair potential in the isotropic effective model. (a) $N = 20$; (b) $N = 50$; (c) $N = 100$. The effective potentials are shown only for r values for which we have relatively good statistics. We also show a sketch of the ↑↑, →→, and ↑→ configurations.

shape fluctuates, they can feel each other also for distances r which are slightly larger than D_{g0}. In the →→ configuration two disks overlap only if the distance between their centers of mass is smaller than their thickness. These results tell us that the peak in the reduced pair correlation function $g(r, \mathbf{d}^{(1)}\cdot\mathbf{d}^{(2)})$ for $r \approx 0.25D_{g0}$ and $\mathbf{d}^{(1)}\cdot\mathbf{d}^{(2)} \approx 1$ is mostly due to →→ like configurations. However, as soon as the rings can overlap in → → type configurations the effective potential increases very fast for smaller r, and we come to a regime where other configurations of the directors are more favorable. As a comparison, we also consider a configuration with $\mathbf{d}^{(1)}\perp\mathbf{d}^{(2)}\|\mathbf{r}$, which we denote by ↑→. The corresponding effective potential is given by

$$\beta V_{\uparrow\rightarrow}(r) = -\ln[g(r,\ \cos\theta_1 = 0,\ \cos\theta_2 = 1,\ \varphi)] \qquad (14)$$

As in the →→ case, the value of the φ coordinate is irrelevant for calculating $V_{\uparrow\rightarrow}(r)$, which we compute from the arithmetic mean of $g(r, \cos\theta_1 = 0, \cos\theta_2 = 1, \varphi)$ in φ.

For small distances r one ring interpenetrates the other in microscopic configurations of type ↑→. While $V_{\uparrow\rightarrow}(r)$ starts to increase at larger r values than $V_{\rightarrow\rightarrow}(r)$, the increase is slower and converges to a constant for $r \to 0$. This is intuitive to understand since it requires only a finite amount of bending energy to deform two rings such that one can fit into the other. The required bending energy is smaller if the rings are larger. The ↑→ becomes dominant over the →→ configuration at an r value below the threshold $r \approx 0.25D_{g0}$. This is also the r value at which we find the transition in the reduced pair correlation function $g(r, \mathbf{d}^{(1)}\cdot\mathbf{d}^{(2)})$ between a regime where configurations with parallel directors, as in →→ , are preferred, to a regime where they are suppressed and other configurations like ↑→ become dominant.

In the Appendix we explain how one can expand the angular part of $g(r, \cos\theta_1, \cos\theta_2, \varphi)$ into a series of suitably chosen basis functions $f_{l_1,l_2,m}(\cos\theta_1, \cos\theta_2, \varphi)$. The expression for this expansion is given in eq 27, and the corresponding coefficients $c_{l_1,l_2,m}(r)$ can be determined by calculating particular ensemble averages as shown in eq 30. We plot these coefficients $c_{l_1,l_2,m}(r)$ for $l_1, l_2 \le 2$ in Figure 5. From the fast change of $c_{l_1,l_2,m}(r)$ for $r \approx 0.25D_{g0}$ one can once more see the transition between two regimes for r in which the distribution of the directors of the ring polymers is very different. We can again see that this transition is smoother for larger rings. The magnitude of

DOI: 10.1021/acs.macromol.5b00603
Macromolecules 2015, 48, 4983−4997

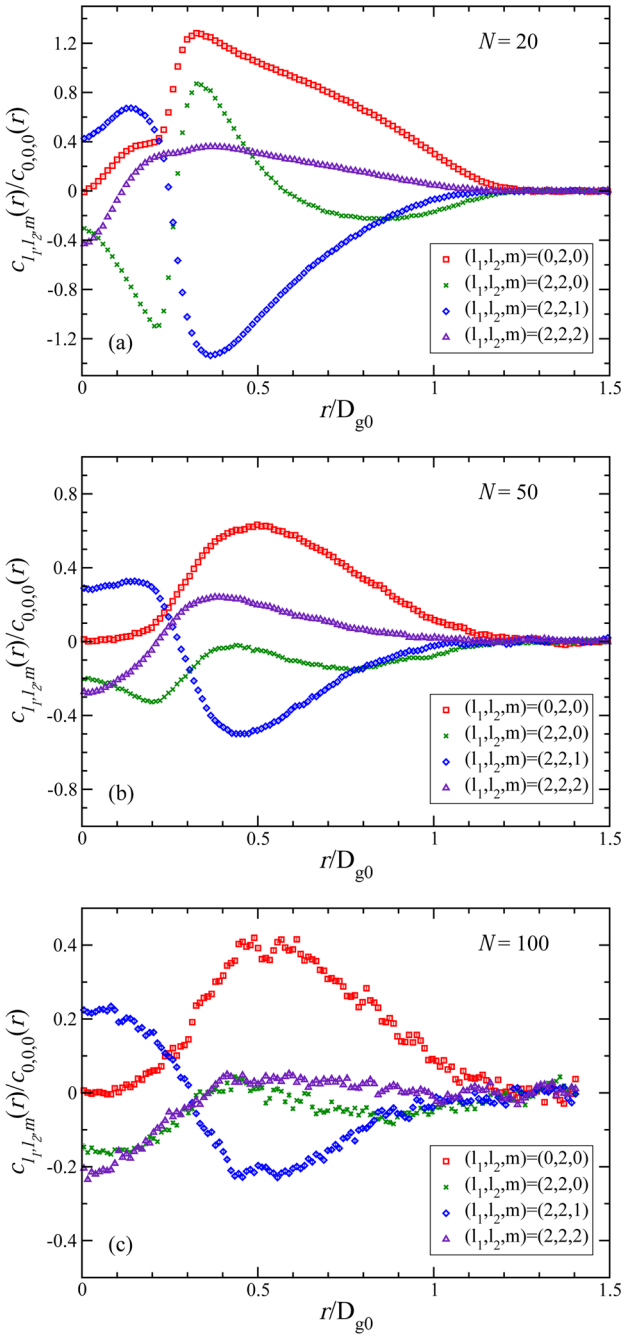

Figure 5. First coefficients in the expansion of $g(r, \cos\theta_1, \cos\theta_2, \varphi)$ divided by the coefficient $c_{0,0,0}(r)$. (a) $N = 20$, (b) $N = 50$, and (c) $N = 100$.

coefficients $c_{l_1,l_2,m}(r)/c_{0,0,0}(r)$ with $(l_1, l_2) \neq (0, 0)$ tells us about the significance of the corresponding anisotropy in $g(r, \cos\theta_1, \cos\theta_2, \varphi)$. Anisotropy is more important for smaller rings and becomes more pronounced after the transition at $r \approx 0.25D_{g0}$, where the rings prefer parallel configurations.

5. MONTE CARLO SIMULATIONS OF THE ANISOTROPIC EFFECTIVE MODEL

We carried out Monte Carlo simulations of systems of effective particles described by the anisotropic effective model for different ring sizes N and various densities. We define the reduced density in our simulation as $\rho^* \equiv nD_{g0}^3/L^3$, where n is the number of rings in the sample. In order to assess the quality of the anisotropic effective model, we compare our results to results of full monomer-resolved simulations from ref 52 and the results of simulations using the isotropic effective model. As we can see in Figure 6 for all choices of the number of monomers N the effective models are in good agreement with the full monomer-resolved simulations at low densities ρ^*. This is an important consistency check for the effective models, in which the interactions have been chosen such that the distribution of the effective degrees of freedom agrees with their distribution in the full monomer-resolved simulations, in the limit of small densities.

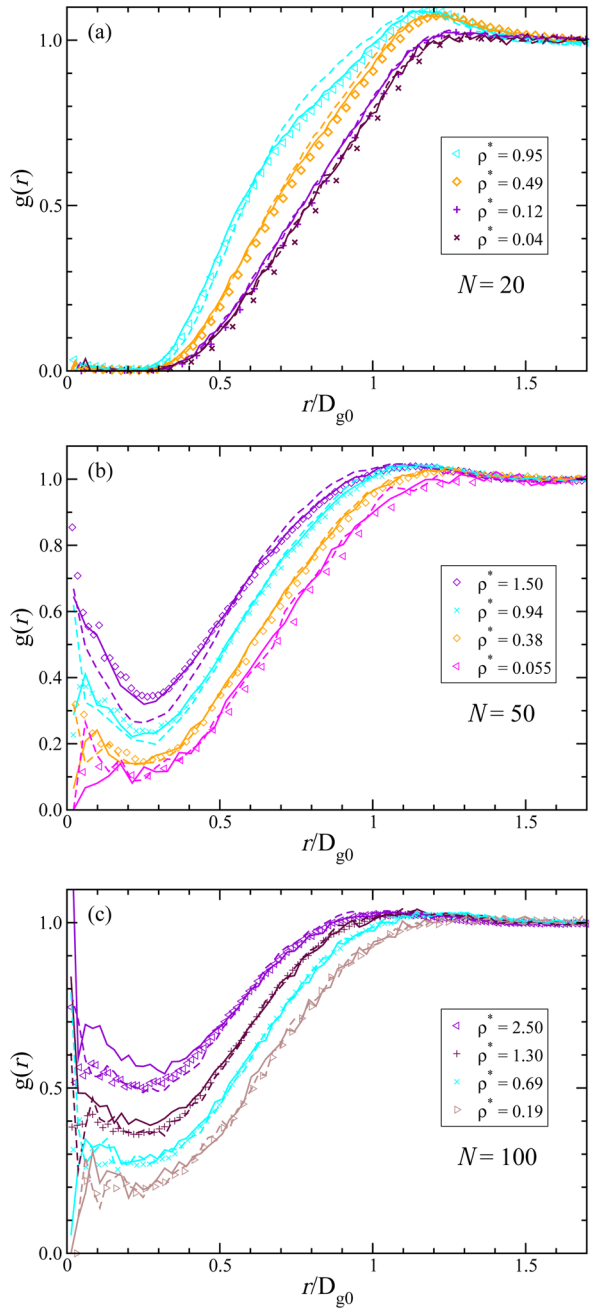

Figure 6. Pair correlation function $g(r)$ at low reduced densities ρ^* for a simulation of many ring polymers in the full monomer-resolved simulation (symbols), the anisotropic effective model (solid line), and the isotropic effective model (dashed line).

DOI: 10.1021/acs.macromol.5b00603
Macromolecules 2015, 48, 4983−4997

In Figure 7, we present results for the smallest rings with $N = 20$ monomers at higher densities. There is a dramatic

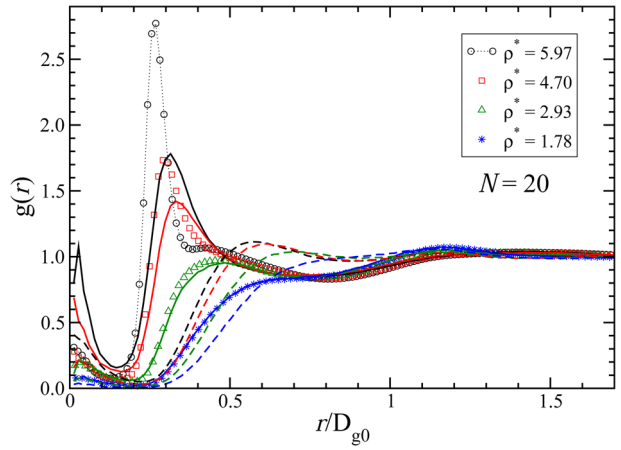

Figure 7. Pair correlation function $g(r)$, at high densities, for a simulation of many ring polymers with $N = 20$ monomers in the full monomer-resolved simulation (symbols), the anisotropic effective model (solid line), and the isotropic effective model (dashed line).

improvement of the accuracy as one compares the isotropic with the anisotropic model. While the former fails for $\rho^* > 2$ the anisotropic effective model works up to $\rho^* \cong 5$ and even gives a semiquantitatively correct description of the system at $\rho^* = 5.97$. At the highest densities, we see the development of a peak in g(r) at $r \cong 0.3D_{g0}$. This peak in the pair correlation function is associated with the emergence of stacks of parallel rings, and its position describes the typical distance of rings in these stacks.[52] Interestingly, the isotropic effective potential has a *maximum* for $r \approx 0.25D_{g0}$, which is close to the typical distance of the rings in the stacks, and one could wonder why the rings prefer to align at a distance which seems to have a very high free energy penalty according to the isotropic effective potential. The answer to this apparent paradox lies in the strongly peaked nature of the anisotropic effective interaction, which we could observe in Figures 3, 4, and 5. While the average configuration of the angular degrees of freedom at distances $r \approx 0.3D_{g0}$ has a high free energy penalty, a certain class of configurations, where the directors of the rings are almost parallel, is much more favorable. Obviously, stacking can not be observed in the isotropic effective model, where particles possess no directional degrees of freedom.

As a further characteristic of the short-range coordination of the rings, we consider the average number $\langle n_r \rangle$ of neighbors within a distance r from the center of mass of a randomly chosen ring. This is expressed as

$$\langle n_r \rangle = 4\pi\rho \int_0^r \mathrm{d}x\, x^2 g(x) \tag{15}$$

For the rings with $N = 20$ monomers we present results for $\langle n_r \rangle$ in Figure 8. Once more, the good agreement between the full monomer-resolved and the anisotropic effective model, even at the highest densities investigated, is confirmed: small differences appear only for $0.25D_{g0} \leq r \leq 0.4D_{g0}$. Evidently, $\langle n_r \rangle$ does not contain more information than the $g(r)$ plot in Figure 7, but it nevertheless clarifies the meaning of the disagreement between the $g(r)$ curves in the monomer-resolved and the anisotropic effective model. At the highest densities in the full simulation, the centers of mass move a bit closer to each other

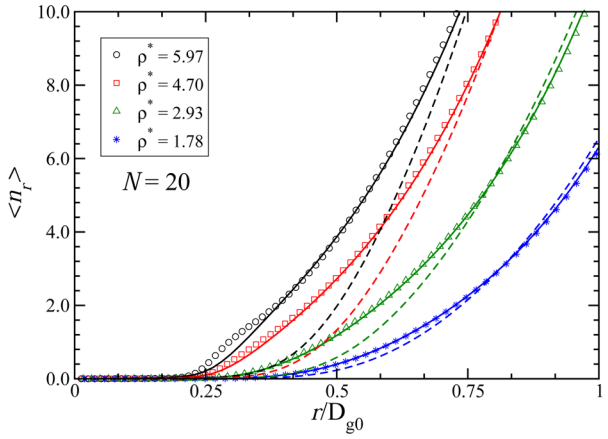

Figure 8. $\langle n_r \rangle$ in a simulation of many ring polymers with $N = 20$ monomers in the full monomer-resolved simulation (symbols), the anisotropic effective model (solid line), and the isotropic effective model (dashed line).

than they do in the anisotropic effective simulation. This manifests itself as a shift of the peaks in the $g(r)$ curves. The difference in the height of the peaks is partly a consequence of the shift, since a peak in $g(r)$ has to be higher at smaller distances if it amounts to the same amount of average neighbors as a peak at a larger distance r. The fact that the $\langle n_r \rangle$ curves for the anisotropic effective and the full simulation in Figure 8 agree for $r \geq 0.4D_{g0}$ shows us that the peaks in the $g(r)$ curves indeed correspond to the same amount of average nearby particles that are simply accumulated at slightly different distances.

We proceed now with the longer rings, $N = 50$. As can be seen by the pair correlation curves in Figure 9a, also in this case the inclusion of anisotropy improves the agreement with the monomer-resolved simulations significantly for densities ρ^* from 2.3 to 10.2. In Figure 9b we present $g(r)$ for higher ρ^*. In the full monomer-resolved simulations we can see a peak emerging in the pair correlation function $g(r)$ at $r = 0$ on increasing the density. As described in refs 52 and 58, the monomer-resolved system forms stacks of quasi-parallel oblate rings that are fully penetrated by bundles of elongated rings. In this phase, the deformation of the penetrating rings is particularly strong. The effective description, on the other hand, breaks down if the internal configurations of the rings in the monomer-resolved system differ significantly to the internal configurations in the system with only two ring polymers. Therefore, the anisotropic effective model should not be expected to be a quantitative description at the high densities in which this phase is formed. Agreement with the monomer-resolved model here is less satisfactory but the improvement over the isotropic model is still spectacular.

For the rings with $N = 100$ we find that anisotropy does not play a key role any more, at least not for the full model at the investigated densities. This had to be expected, as we could already see in Figure 3 and 5 that anisotropy is less pronounced for larger ring sizes. As we saw in Figure 6c, both the isotropic and the anisotropic model give good results for $g(r)$ up to $\rho^* \approx 2.5$. In Figure 10, we see that for higher densities the inclusion of anisotropy does not yield results that are in better agreement with the full monomer-resolved simulations. The results in the isotropic effective model even seem to be in better agreement with the full model, which is attributed to multiparticle interactions that can change the configurations of the large

DOI: 10.1021/acs.macromol.5b00603
Macromolecules 2015, 48, 4983−4997

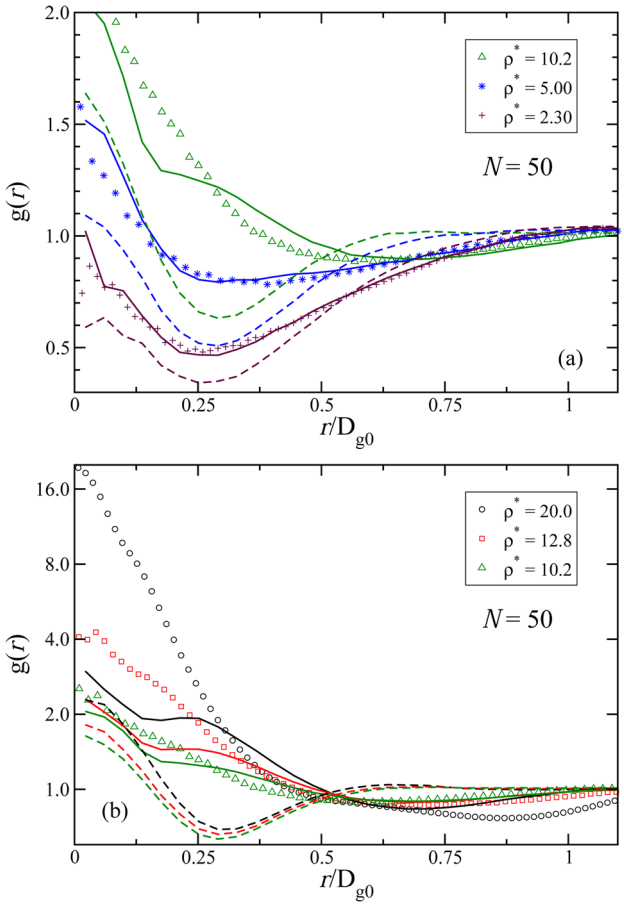

Figure 9. Pair correlation function $g(r)$ for a simulation of many ring polymers with N = 50 monomers in the full monomer-resolved simulation (symbols), the anisotropic effective model (solid line), and the isotropic effective model (dashed line). The two plots show different reduced density ρ^* ranges.

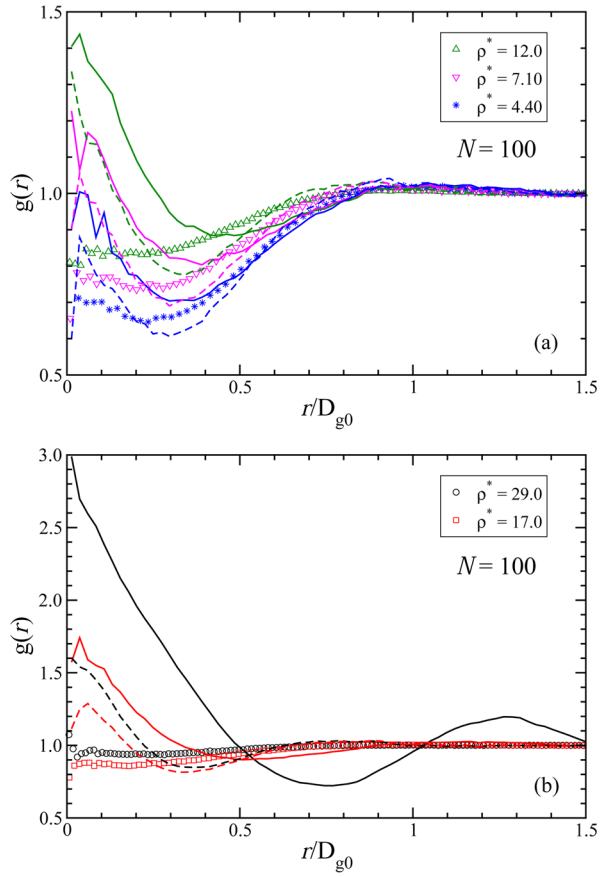

Figure 10. Pair correlation function $g(r)$ for a simulation of many ring polymers with N = 100 monomers in the full monomer-resolved simulation (symbols), the anisotropic effective model (solid line), and the isotropic effective model (dashed line). The two plots show different reduced density ρ^* ranges.

and therefore more deformable rings significantly. The already small correlation between the directors, which is present in the dilute case, might therefore be even smaller at high densities. In the anisotropic effective model, we then overestimate the angular correlations between the directors and arrive at results that can be slightly worse than those of the isotropic model. Interestingly, at ρ^* = 20.0, which is the highest density investigated, the anisotropic model appears to crystallize. At this density we see the emergence of columns that are closed over the periodic boundary conditions and organize in a hexagonal 2D lattice structure.

Finally, let us focus exclusively on orientational correlations. We define $P(\mathbf{d}^{(1)}\cdot\mathbf{d}^{(2)})$ as the probability density distribution for the scalar products between the directors $\mathbf{d}^{(1)}$ and $\mathbf{d}^{(2)}$ of two ring polymers which are a distance $r < 0.6D_{g0}$ away from each other. In Figure 11, we present results for $P(\mathbf{d}^{(1)}\cdot\mathbf{d}^{(2)})$ for simulations in the monomer resolved and in the anisotropic effective model. If the directors were uncorrelated, $P(\mathbf{d}^{(1)}\cdot\mathbf{d}^{(2)})$ would be equal to 1. For low densities ρ^* we obtain good agreement for all ring sizes investigated. Since we only look at the directional correlation of close by ring polymers, $P(\mathbf{d}^{(1)}\cdot\mathbf{d}^{(2)})$ can show strong anisotropic features even for $\rho^* \to 0$. As expected, the anisotropy in $P(\mathbf{d}^{(1)}\cdot\mathbf{d}^{(2)})$ is stronger for smaller rings. When the density is increased, the distribution always shifts toward parallel configurations in the effective model. This happens because less volume per ring is available for higher ρ^* and by aligning parallel the rings occupy less space. Typically one observes the same trend in the monomer-resolved simulation; only for the N = 100 rings we find more parallel rings for ρ^* = 2.5 than for ρ^* = 17.0. In contrast to the effective model the rings in the monomer-resolved simulation can deform, and their interaction with other rings can therefore be more isotropic at higher densities ρ^*. This explains why for the large rings with N = 100 monomers, which deform more easily than the smaller rings, the correlation between the directors is much weaker than in the effective model and can even decrease with density. For N = 50 one can see that the number of orthogonal rings in the monomer-resolved model at high densities is significantly larger than in the effective simulation. As described in refs 52 and 58 for N = 50 and $\rho^* \geq 12.8$ one observes that oblate rings are interpenetrated by elongated prolate rings. Since the directors of the oblate and the interpenetrating prolate rings can be orthogonal to each other, one observes perpendicular directors for N = 50 even at the highest densities investigated. In the anisotropic effective model, on the other hand, this interpenetration is disfavored, and we observe almost no orthogonal close-by rings at ρ^* = 20 for N = 50.

6. TRUNCATION OF THE EXPANSION OF THE ANISOTROPIC POTENTIAL

Instead of working with a fully tabulated effective potential on a four-dimensional grid, it can be advantageous to use the

DOI: 10.1021/acs.macromol.5b00603
Macromolecules 2015, 48, 4983−4997

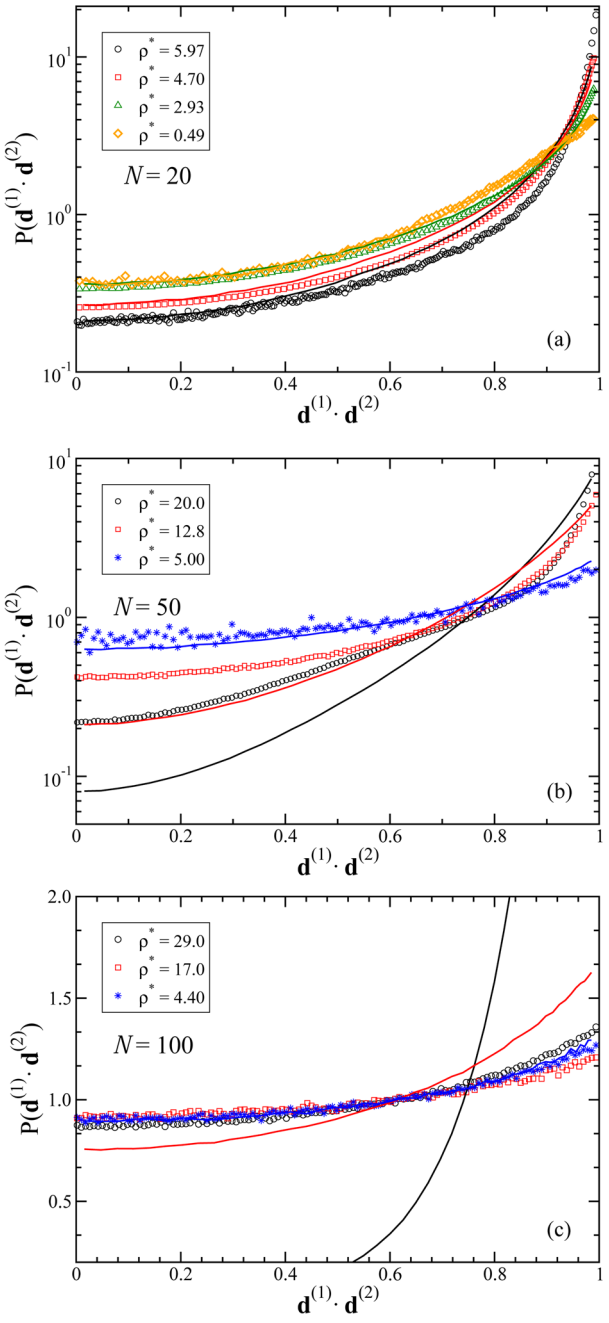

Figure 11. $P(\mathbf{d}^{(1)}\cdot\mathbf{d}^{(2)})$ is the probability density to find the scalar product $\mathbf{d}^{(1)}\cdot\mathbf{d}^{(2)}$ between the directors of two close by rings ($r < 0.6D_{g0}$). Here we show $P(\mathbf{d}^{(1)}\cdot\mathbf{d}^{(2)})$ for a simulation of many ring polymers in the full monomer-resolved simulation (symbols) and the anisotropic effective model (solid line). (a) $N = 20$, (b) $N = 50$, and (c) $N = 100$.

analytical expansion on basis functions presented in the Appendix. Such expansions are truncated after some term, and here we shortly discuss the quality of such truncations for the problem at hand. To test the quality of the expansion of $g(r, \cos\theta_1, \cos\theta_2, \varphi)$ we also carried out Monte Carlo simulations, where we used the effective potential associated with the expanded correlation function as the pair interaction between our effective particles. We took the 14 coefficients $c_{l_1,l_2,m}(r)$ for which $l_1, l_2 \leq 4$ into account and truncated the rest of the expansion. While $g(r, \cos\theta_1, \cos\theta_2, \varphi)$ can never be negative, the truncated expanded version of g can accidentally become smaller than zero. Wherever this happens $g = 0$ and $V_{\text{eff}} = \infty$ are used in the simulation. In Figure 12 the pair correlation

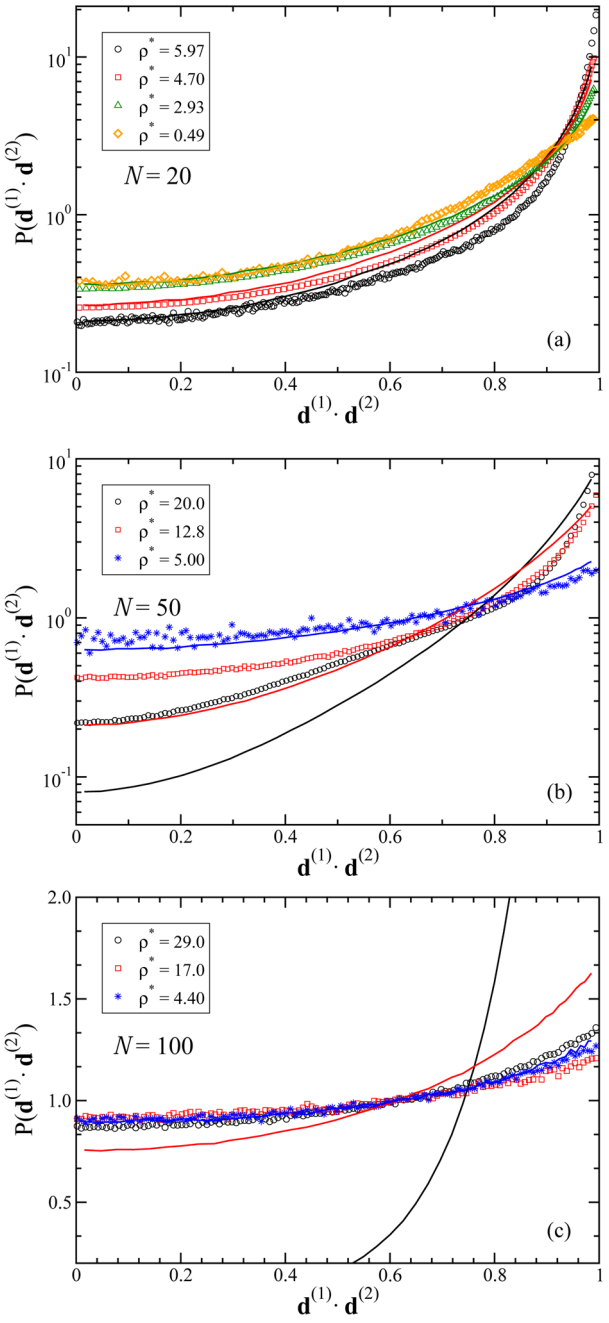

Figure 12. Pair correlation function $g(r)$ for a simulation of many ring polymers in the anisotropic effective model. For the dashed line we expanded the pair-correlation function g before computing the associated effective pair potential. For the expansion we took the 14 coefficients for which $l_1, l_2 \leq 4$ into account. The solid line shows results of a simulation with the unexpanded effective pair interaction. (a) $N = 20$ and (b) $N = 50$.

function $g(r)$ obtained in this simulation is shown in comparison with the $g(r)$ function, which we computed previously employing the full anisotropic effective potential. For both $N = 20$ and $N = 50$ we obtain reasonable results with the truncated effective interaction, given by only 14 expansion coefficients. For the full effective interaction, which we store on a 4D grid, we save $16^3 = 4096$ entries for each value of r (see

DOI: 10.1021/acs.macromol.5b00603
Macromolecules 2015, 48, 4983−4997

section 3.1). At intermediate densities the results obtained with the expanded effective interaction are a significant improvement with respect to the isotropic effective model. However, one has to be aware that for $N = 20$ the coefficients of higher order modes can still be quite high, especially for r between $0.2D_{g0}$ and $0.7D_{g0}$. In Figure 5 we see that the coefficient for the mode with $(l_1, l_2, m) = (0, 2, 0)$ can be larger than the coefficient of the isotropic expansion mode. The reason for the high contribution of higher order modes for $N = 20$ is of course the strongly peaked nature of $g(r, \cos\theta_1, \cos\theta_2, \varphi)$ for these small rings, which we can also observe in Figure 3. The convergence of $g(r, \cos\theta_1, \cos\theta_2, \varphi)$ is poor for the $N = 20$ rings due to the strong anisotropy of their effective interaction. However, our results show that the expansion modes up to $l_1, l_2 \leq 4$ already capture the main features of the effective interaction. For $N = 50$ the degree of anisotropy is weaker, and therefore the convergence of the expansion of $g(r, \cos\theta_1, \cos\theta_2, \varphi)$ is better.

7. CONCLUSIONS

We have introduced a minimal anisotropic model to coarse-grain ring polymers with a finite bending rigidity as soft, penetrable disks. For the shortest ($N = 20$) and the intermediate ($N = 50$) sized rings, this model represents a dramatic improvement over the isotropic coarse-graining, in which the relative orientations between the rings are all integrated upon and a radially symmetric interaction results instead. The approach is capable of distinguishing between the relative orientations at infinite dilution, and it carries this distinction also to highly concentrated systems, where it reproduces well the salient features of the structure as seen in the full monomer-resolved simulations. Whereas this is valid more for $N = 20$ and $N = 50$, which have a contour length to persistence length ratio of $N/s_p \sim 2.7$ and 6.7, respectively, some important features, such as the penetration of elongated rings in columns formed by oblate rings (found for $N = 50$), are suppressed or even lost in the effective description, as genuine many-body effects come into play. For the largest rings, $N = 100$, for which we obtain $N/s_p \sim 13.3$, the contour length is much larger than the persistence length, and they thus resemble more flexible objects. In this case the anisotropic potential at high concentrations fails to describe the structural correlations. This indeed reflects the fact that such rings undergo, at high concentrations, conformational changes (shrinking, interpenetration) that are quite distinct from the assumptions that go into the anisotropic, soft disk model, rendering it thereby very inaccurate. We therefore expect that our anisotropic model yields quantitative results over a broad density range, for systems of polymer rings with a contour to persistence length ratio of $N/s_p \lesssim 10$.

Our work provides, thus, an accurate and efficient general scheme for the coarse-graining of semiflexible ring polymers, as it allows for a very dramatic reduction of their degrees of freedom, while at the same time introducing a realistic class of systems for which anisotropic generalizations of the ultrasoft, penetrable effective interactions are physically meaningful. Future work will focus on the investigations of the structural and phase behavior of mixtures of stiff rings and of the dynamics of the structure formation in the same.

APPENDIX

A. Calculation of the Anisotropic Effective Potential

As discussed in section 2, we wish to sample $P(r, \cos\theta_1, \cos\theta_2, \varphi)$ for a system of two ring polymers, in order to obtain a numerical expression for the anisotropic effective potential between them. We know that for large values of r, when the polymers cannot interact with each other, P will correspond to the ideal case, P_{id}. Therefore, the interesting configurations for us are those values of r that result in overlaps between the ellipsoids of gyration. We use a biasing potential between the centers of mass of the two rings to restrict r to certain *umbrella windows*:

$$V_{\text{bias}}^{(j)}(r) = \frac{k_j}{2}(r - r_j)^2 \tag{16}$$

With r_j and k_j we can tune respectively the location and width of the window for r in which configurations are sampled. We carry out simulations for a range of different r_j and k_j values and calculate histograms $P_{\text{bias}}^{(j)}(Q)$ in the effective coordinates. Here, Q stands for $(r, \cos\theta_1, \cos\theta_2, \varphi)$ as a collective variable and thus denotes a bin in the effective coordinates, whereas j is the index of the respective biased simulation and thus determines k_j and r_j. The binning in the 4D space is identical for all biased simulations. We use the self-consistent histogram method by Ferrenberg and Swendsen[64,65] to combine the different $P_{\text{bias}}^{(j)}(Q)$, which results in an estimate $P_{\text{est},j}(Q)$ for the histogram $P(Q)$ of the unbiased system. The starting point of this method is that every simulation does in principle give an estimate for the histogram $P(Q)$ of the unbiased simulation:

$$P_{\text{est},j}(Q) = N^{(j)} \exp(\beta V_{\text{bias}}^{(j)}(Q)) P_{\text{bias}}^{(j)}(Q) \tag{17}$$

Here, $V_{\text{bias}}^{(j)}$ denotes the bias potential in the jth simulation, given by (16), and $N^{(j)}$ is a normalization factor, which can be expressed as

$$N^{(j)} = \sum_Q P(Q) \exp(-\beta V_{\text{bias}}^{(j)}(Q)) \tag{18}$$

assuming that both $P(Q)$ and $P_{\text{bias}}^{(j)}(Q)$ are normalized. However, this estimate for $P(Q)$ will only be useful for Q bins that have good statistics in the jth simulation, which in our case means that the bins are at an r coordinate that is close to the r_j value of the respective bias. Another problem with this expression is that in order to calculate $N^{(j)}$ we already need to know the sought-for quantity $P(Q)$. To deal with the first problem, we combine the individual estimates obtained from each jth simulation, to form an improved estimate:

$$P_{\text{est}}(Q) = \sum_j c^{(j)}(Q) P_{\text{est},j}(Q) \tag{19}$$

With $c^{(j)}(Q)$ we can tune the weight of $P_{\text{est},j}(Q)$ in the $P(Q)$ estimate. We require $\sum_j c^{(j)}(Q) = 1$. In bins where the jth simulation has bad statistics we will choose $c^{(j)}(Q)$ close to 0, such that the $P_{\text{est},j}(Q)$ estimate contributes only in bins where it is useful. The error of $P_{\text{est}}(Q)$ can be estimated via the Poisson distribution, and it can be minimized via the following choice for the $c^{(j)}(Q)$:

$$c^{(j)}(Q) = \frac{\exp(-\beta V_{\text{bias}}^{(j)}(Q)) M^{(j)} N^{(j)}}{\sum_k \exp(-\beta V_{\text{bias}}^{(k)}(Q)) M^{(k)} N^{(k)}} \tag{20}$$

DOI: 10.1021/acs.macromol.5b00603
Macromolecules 2015, 48, 4983−4997

Here $M^{(j)}$ is the number of uncorrelated configurations sampled in the jth simulation. With eqs 17−20 we now arrive at an expression for an estimate of $P(Q)$. However, as $N^{(j)}$ depends on $P(Q)$, expression 18 can only be evaluated if $P(Q)$ is known in the first place. We can deal with this problem by using $P_{est}(Q)$ for $P(Q)$ in the formula for $N^{(j)}$ (18) to obtain a self-consistency problem for $P_{est}(Q)$, which can be solved iteratively. As a starting point for this iterative procedure an initial guess for $P_{est}(Q)$ has to be provided. However, after many iterations the procedure is expected to converge to the same distribution, independent of the given initial condition. We started the iterative algorithm with an uniform distribution for $P_{est}(Q)$.

B. Expansion of $g(r, \cos\theta_1, \cos\theta_2, \varphi)$

As the anisotropic effective potential $V_{eff}(r, \cos\theta_1, \cos\theta_2, \varphi)$ and the corresponding pair-correlation function $g(r, \cos\theta_1, \cos\theta_2, \varphi)$ depend on four variables, it is hard to visualize them. Nevertheless, we can obtain a quantitative measure of the anisotropy in g and V_{eff} by carrying out an expansion of g:

$$g(r, \cos\theta_1, \cos\theta_2, \varphi) = \sum_n c_n(r) f_n(\cos\theta_1, \cos\theta_2, \varphi) \tag{21}$$

Here, f_n are modes that depend on the angular degrees of freedom only, and they form a complete basis for the angular dependence of g.

To obtain a suitable set of basis functions f_n for the dependence of g on the directors $\mathbf{d}^{(1,2)}$ for a given vector $\mathbf{r}$ between the rings, we started with an expansion to a sum of products of spherical harmonics:

$$\gamma(\mathbf{d}^{(1)}, \mathbf{d}^{(2)}) = \sum_{l_1=0}^{\infty} \sum_{m_1=-l_1}^{l_1} \sum_{l_2=0}^{\infty} \sum_{m_2=-l_2}^{l_2} c_{l_1,m_1,l_2,m_2} Y_{l_1}^{m_1}(\cos\theta_1, \varphi_1) Y_{l_2}^{m_2}(\cos\theta_2, \varphi_2) \tag{22}$$

Here γ denotes g at a given $\mathbf{r}$. By $\cos\theta_i$ and φ_i the director $\mathbf{d}^{(i)}$ is represented in spherical coordinates. We use a reference frame where the connection vector $\mathbf{r}$ between the two rings points to the north pole, and therefore φ_i denotes the azimuthal angle around $\mathbf{r}$. With Y_l^m we denote the spherical harmonics.[66] They fulfill the orthonormality relation $\int d\Omega\ \overline{Y}_l^m(\cos\theta,\varphi)\ Y_{l'}^{m'}(\cos\theta,\varphi) = \delta_{l,l'}\delta_{m,m'}$ with $d\Omega = d\cos\theta\, d\varphi$, where $\bar{z}$ denotes the complex conjugation of a complex number z. This allows us to compute the expansion coefficients via integration:

$$c_{l_1,m_1,l_2,m_2} = \int d\Omega_1\, d\Omega_2\, \overline{Y}_{l_1}^{m_1}(\cos\theta_1, \varphi_1) \overline{Y}_{l_2}^{m_2}(\cos\theta_2, \varphi_2)\ \gamma(\cos\theta_1, \varphi_1, \cos\theta_2, \varphi_2) \tag{23}$$

Due to the symmetries of γ, we will now be able to compute or relate many of the coefficients and thus arrive at a reduced set of basis functions $\{f_{l_1,l_2,m}\}$ with which we can still represent γ exactly. We first use the continuous symmetry under rotations around the connection vector $\mathbf{r}$:

$$\gamma(\cos\theta_1, \varphi_1, \cos\theta_2, \varphi_2) = \gamma(\cos\theta_1, \varphi_1 - \varphi_2, \cos\theta_2, 0) \tag{24}$$

Using eq 23 and $Y_l^m(\cos\theta, \varphi) \propto \exp(im\varphi)$, one can show that c_{l_1,m_1,l_2,m_2} vanishes for $m_1 \neq -m_2$ due to this symmetry. In the following, we enumerate the expansion modes with $m \equiv m_1 = -m_2$. Next we use that $\mathbf{d}^{(i)}$ is equivalent to $-\mathbf{d}^{(i)}$, and therefore γ fulfills the symmetry $\gamma(\mathbf{d}^{(1)},\mathbf{d}^{(2)}) = \gamma(-\mathbf{d}^{(1)},\mathbf{d}^{(2)}) = \gamma(\mathbf{d}^{(1)},-\mathbf{d}^{(2)})$. Since $Y_l^m(\mathbf{d}) = (-1)^l\, Y_l^m(-\mathbf{d})$, c_{l_1,m_1,l_2,m_2} are zero if either l_1 or l_2 is odd.

The monomer-resolved model is symmetric under a mirror transformation, which is therefore also a symmetry of the effective model. If we consider a state with $\varphi_2 = 0$ and mirror it by a plane spanned by $\mathbf{r}$ and $\mathbf{d}^{(2)}$, we obtain a state with identical $\mathbf{r}$, $\mathbf{d}^{(2)}$, and $\cos\theta_1$, while φ_1 changes sign. Hence, we obtain

$$\begin{aligned}\gamma(\cos\theta_1, \varphi_1, \cos\theta_2, \varphi_2) &= \gamma(\cos\theta_1, \varphi_1 - \varphi_2, \cos\theta_2, 0)\\ &= \gamma(\cos\theta_1, \varphi_2 - \varphi_1, \cos\theta_2, 0)\\ &= \gamma(\cos\theta_1, \varphi_2, \cos\theta_2, \varphi_1)\end{aligned} \tag{25}$$

For the first and the last step we used (24). Therefore, γ is invariant under exchanging φ_1 and φ_2. We therefore have $c_{l_1,m,l_2,-m} = c_{l_1,-m,l_2,m}$.

Everything discussed so far also holds if we calculate the effective interaction between different rings, e.g., for rings with a different number of monomers. The final symmetry, which we will exploit now, only holds if we have identical rings. In this case we obtain an equivalent state if we swap the orientations of the two ring polymers:

$$\begin{aligned}\gamma(\cos\theta_1, \varphi_1, \cos\theta_2, \varphi_2) &= \gamma(\cos\theta_2, \varphi_2, \cos\theta_1, \varphi_1)\\ &= \gamma(\cos\theta_2, \varphi_1, \cos\theta_1, \varphi_2)\end{aligned} \tag{26}$$

For the last transformation we used (25). Hence, for identical rings γ is also invariant under an exchange of θ_1 and θ_2, and we therefore know that $c_{l_1,m,l_2,-m} = c_{l_2,m,l_1,-m}$.

We now group basis functions if we *a priori* know that γ has identical coefficients $c_{l_1,m,l_2,-m}$ with respect to them. We sum the modes in each group and divide by $\sqrt{\#}$, where # is the number of modes in the group. For identical rings # is at most 4 but can also be smaller if $l_1 = l_2$ or $m = 0$. For different rings # = 2 if $m \neq 0$ and 1 otherwise. In this way we obtain a new set of basis functions $f_{l_1,l_2,m}$. The indices of $f_{l_1,l_2,m}$ refer to the indices of one of the modes in the group from which $f_{l_1,l_2,m}$ was constructed, with the additional constraint that $m \geq 0$ and $l_2 \geq l_1$ in the case of identical rings. As an example, we can consider $f_{2,4,1}$, which is set to $(Y_2^1\, Y_4^{-1} + Y_2^{-1}\, Y_4^1 + Y_4^1\, Y_2^{-1} + Y_4^{-1}\, Y_2^1)/\sqrt{4}$ in the case of identical and $(Y_2^1\, Y_4^{-1} + Y_2^{-1}\, Y_4^1)/\sqrt{2}$ in the case of different rings. The new basis functions $f_{l_1,l_2,m}$ only depend on $\varphi \equiv |\varphi_1 - \varphi_2|$ and not on φ_1 and φ_2 separately. Thus, $|\varphi_1 - \varphi_2|$ is precisely the φ coordinate defined in (6), on which g depends. Expanding the angular dependence of g with our new basis functions, we obtain

$$g(r, \cos\theta_1, \cos\theta_2, \varphi) = \sum_{l_1=\{0,2,4,\ldots\}} \sum_{l_2=\{l_1,l_1+2,l_1+4,\ldots\}} \sum_{m=0}^{\min(l_1,l_2)} c_{l_1,l_2,m}(r) f_{l_1,l_2,m}(\cos\theta_1, \cos\theta_2, \varphi) \tag{27}$$

In the case of different rings, the sum over l_2 does not start at l_1 but at 0. Like $\{Y_{l_1}^m Y_{l_2}^{-m}\}$, also $\{f_{l_1,l_2,m}\}$ fulfill the orthonormality relation

$$\int d\Omega_1\, d\Omega_2\, f_{l_1,l_2,m}(\cos\theta_1, \cos\theta_2, \varphi)\ f_{l'_1,l'_2,m'}(\cos\theta_1, \cos\theta_2, \varphi) = \delta_{l,l'}\delta_{m,m'} \tag{28}$$

DOI: 10.1021/acs.macromol.5b00603
Macromolecules 2015, 48, 4983−4997

Note that complex conjugation is not necessary as $f_{l_1,l_2,m}$ are real functions in contrast to $Y_{l_1}^{m}Y_{l_2}^{-m}$. Hence, we can obtain the coefficients $c_{l_1,l_2,m}(r)$ via an integration analogous to (23):

$$c_{l_1,l_2,m}(r) = \int \mathrm{d}\Omega_1\, \mathrm{d}\Omega_2\, f_{l_1,l_2,m}(\cos\theta_1,\ \cos\theta_2,\ \varphi)\, g(r,\ \cos\theta_1,\ \cos\theta_2,\ \varphi) \tag{29}$$

To calculate $c_{l_1,l_2,m}(r)$, we could do a numerical integration of $g(r, \cos\theta_1, \cos\theta_2, \varphi)$. A different approach for the calculation of $c_{l_1,l_2,m}(r)$ is to express the integral in (29) as an average over configurations of a system of two ring polymers for fixed r. We sample these configurations from the simulations with the bias potential $V_{\mathrm{bias}}(r)$ given in (16), which we carried out for calculating g on a 4D grid using *umbrella sampling*. As $V_{\mathrm{bias}}(r)$ does not change the relative weight of configurations with identical r values, we can use the configurations that fall in a small window of r values to estimate averages over the angular degrees of freedom at some fixed r value. The average of the expansion modes $f_{l_1,l_2,m}$ over the configurations of the rings is related to $c_{l_1,l_2,m}(r)$ as follows:

$$\langle f_{l_1,l_2,m}\rangle_r = \frac{\int \mathrm{d}\Omega_1\, \mathrm{d}\Omega_2\, g(r,\ \cos\theta_1,\ \cos\theta_2,\ \varphi)\, f_{l_1,l_2,m}(\cos\theta_1,\ \cos\theta_2,\ \varphi)}{\int \mathrm{d}\Omega_1\, \mathrm{d}\Omega_2\, g(r,\ \cos\theta_1,\ \cos\theta_2,\ \varphi)} = \frac{c_{l_1,l_2,m}(r)}{(4\pi)^2 g^{\mathrm{iso}}(r)} \tag{30}$$

Here we used (9) and (29) for the final step. g^{iso} is easy to calculate numerically once we know g. The advantage of this approach with respect to a numerical evaluation of (29) is that we do not need to introduce a grid in the angular degrees of freedom. In particular, if we want to calculate $c_{l_1,l_2,m}(r)$ coefficients for high l_1 and l_2 values, the correctness of the result in the first approach depends sensitively on the number of grid points and also on the numerical method for carrying out the integration. Calculating averages, on the other hand, is straightforward, and we can easily estimate the statistical error using the standard deviation of block averages. For these reasons we calculate the expansion coefficients $c_{l_1,l_2,m}(r)$ and estimate their errors following the latter approach.

The larger l_i, the faster the $f_{l_1,l_2,m}$ functions can change when the director $\mathbf{d}^{(i)}$ is varied. $f_{0,0,0} = (4\pi)^{-1}$ is constant and therefore gives the isotropic contribution. By comparing $c_{0,0,0}(r)$ with the size of the coefficients for $(l_1, l_2, m) \neq (0, 0, 0)$ we can quantify the importance of anisotropy in the effective interaction.

We find that with the 14 coefficients $c_{l_1,l_2,m}(r)$ for which $l_1, l_2 \leq 4$ we already get a reasonable approximation of g. This is true, even for the smallest rings investigated ($N = 20$), where the anisotropy is most important. This fact allows us to store the essential information in the anisotropic potential with only a few functions of one variable, $c_{l_1,l_2,m}(r)$, instead of a 4D grid with a very large number of grid points. Using only the coefficient $c_{0,0,0}(r)$, we recover $g^{\mathrm{iso}}(r)$ of the isotropic effective model.

AUTHOR INFORMATION

Corresponding Author

*E-mail: peter.poier@univie.ac.at (P.P.).

Notes

The authors declare no competing financial interest.

ACKNOWLEDGMENTS

This work has been supported by the Austrian Science Fund (FWF), Grant 23400-N16.

REFERENCES

(1) Micheletti, C.; Marenduzzo, D.; Orlandini, E. *Phys. Rep.* **2011**, *504*, 1−73.
(2) Adams, C. C. *The Knot Book*; American Mathematical Society: Providence, RI, 1994.
(3) Tubiana, L.; Orlandini, E.; Micheletti, C. *Prog. Theor. Phys. Supplement* **2011**, *191*, 192−204.
(4) Grosberg, A. Y.; Rabin, Y. *Phys. Rev. Lett.* **2007**, *99*, 217801.
(5) Matthews, R.; Louis, A. A.; Likos, C. N. *ACS Macro Lett.* **2012**, *1*, 1352−1356.
(6) Poier, P.; Likos, C. N.; Matthews, R. *Macromolecules* **2014**, *47*, 3394−3400.
(7) Dai, L.; Renner, C. B.; Doyle, P. S. *Macromolecules* **2014**, *47*, 6135−6140.
(8) Di Stefano, M.; Tubiana, L.; Di Ventra, M.; Micheletti, C. *Soft Matter* **2014**, *10*, 6491−6498.
(9) Renner, C. B.; Doyle, P. S. *ACS Macro Lett.* **2014**, *3*, 963−967.
(10) Micheletti, C.; Orlandini, E. *ACS Macro Lett.* **2014**, *3*, 876−880.
(11) Dai, L.; Renner, C. B.; Doyle, P. S. *Phys. Rev. Lett.* **2015**, *114*, 037801.
(12) Sogo, J. M.; Stasiak, A.; Martınez-Robles, M. L.; Krimer, D. B.; Hernández, P.; Schvartzman, J. B. *J. Mol. Biol.* **1999**, *286*, 637−643.
(13) Arsuaga, J.; Vázquez, M.; Trigueros, S.; Sumners, D. W.; Roca, J. *Proc. Natl. Acad. Sci. U. S. A.* **2002**, *99*, 5373−5377.
(14) Portugal, J.; Rodríguez-Campos, A. *Nucleic Acids Res.* **1996**, *24*, 4890−4894.
(15) Deibler, R. W.; Mann, J. K.; De Witt, L. S.; Zechiedrich, L. *BMC Mol. Biol.* **2007**, *8*, 44.
(16) Liu, Z.; Deibler, R. W.; Chan, H. S.; Zechiedrich, L. *Nucleic Acids Res.* **2009**, *37*, 661−671.
(17) Des Cloizeaux, J. *J. Phys. (Paris)* **1981**, *42*, 635−652.
(18) Grosberg, A. Y.; Feigel, A.; Rabin, Y. *Phys. Rev. E: Stat. Phys., Plasmas, Fluids, Relat. Interdiscip. Top.* **1996**, *54*, 6618.
(19) Deutsch, J. *Phys. Rev. E: Stat. Phys., Plasmas, Fluids, Relat. Interdiscip. Top.* **1999**, *59*, R2539.
(20) Grosberg, A. Y. *Phys. Rev. Lett.* **2000**, *85*, 3858.
(21) Dobay, A.; Dubochet, J.; Millett, K.; Sottas, P.-E.; Stasiak, A. *Proc. Natl. Acad. Sci. U. S. A.* **2003**, *100*, 5611−5615.
(22) Moore, N. T.; Lua, R. C.; Grosberg, A. Y. *Proc. Natl. Acad. Sci. U. S. A.* **2004**, *101*, 13431−13435.
(23) Moore, N. T.; Grosberg, A. Y. *Phys. Rev. E* **2005**, *72*, 061803.
(24) Mansfield, M. L.; Douglas, J. F. *J. Chem. Phys.* **2010**, *133*, 044903.
(25) De Gennes, P.-G. *Scaling Concepts in Polymer Physics*; Cornell University Press: Ithaca, NY, 1979.
(26) Bohn, M.; Heermann, D. W. *J. Chem. Phys.* **2010**, *132*, 044904.
(27) Narros, A.; Moreno, A. J.; Likos, C. N. *Soft Matter* **2010**, *6*, 2435−2441.
(28) Vettorel, T.; Grosberg, A. Y.; Kremer, K. *Phys. Biol.* **2009**, *6*, 025013.
(29) Halverson, J. D.; Lee, W. B.; Grest, G. S.; Grosberg, A. Y.; Kremer, K. *J. Chem. Phys.* **2011**, *134*, 204904.
(30) Kapnistos, M.; Lang, M.; Vlassopoulos, D.; Pyckhout-Hintzen, W.; Richter, D.; Cho, D.; Chang, T.; Rubinstein, M. *Nat. Mater.* **2008**, *7*, 997−1002.
(31) Halverson, J. D.; Lee, W. B.; Grest, G. S.; Grosberg, A. Y.; Kremer, K. *J. Chem. Phys.* **2011**, *134*, 204905.
(32) Marenduzzo, D.; Orlandini, E. *J. Stat. Mech.: Theory Exp.* **2009**, *2009*, L09002.
(33) Dorier, J.; Stasiak, A. *Nucleic Acids Res.* **2009**, *37*, 6316−6322.

DOI: 10.1021/acs.macromol.5b00603
Macromolecules 2015, 48, 4983−4997

(34) Marenduzzo, D.; Micheletti, C.; Orlandini, E. *J. Phys.: Condens. Matter* **2010**, *22*, 283102.
(35) Likos, C. N. *Phys. Rep.* **2001**, *348*, 267−439.
(36) Likos, C. N. *Soft Matter* **2006**, *2*, 478−498.
(37) Louis, A.; Bolhuis, P.; Hansen, J.; Meijer, E. *Phys. Rev. Lett.* **2000**, *85*, 2522.
(38) Krakoviack, V.; Hansen, J.-P.; Louis, A. *Phys. Rev. E: Stat. Phys., Plasmas, Fluids, Relat. Interdiscip. Top.* **2003**, *67*, 041801.
(39) Narros, A.; Likos, C. N.; Moreno, A. J.; Capone, B. *Soft Matter* **2014**, *10*, 9601−9614.
(40) Likos, C.; Löwen, H.; Watzlawek, M.; Abbas, B.; Jucknischke, O.; Allgaier, J.; Richter, D. *Phys. Rev. Lett.* **1998**, *80*, 4450.
(41) Jusufi, A.; Likos, C. N. *Rev. Mod. Phys.* **2009**, *81*, 1753.
(42) Marzi, D.; Likos, C. N.; Capone, B. *J. Chem. Phys.* **2012**, *137*, 014902.
(43) Capone, B.; Coluzza, I.; LoVerso, F.; Likos, C. N.; Blaak, R. *Phys. Rev. Lett.* **2012**, *109*, 238301.
(44) Jusufi, A.; Likos, C.; Löwen, H. *J. Chem. Phys.* **2002**, *116*, 11011−11027.
(45) Huissmann, S.; Blaak, R.; Likos, C. N. *Macromolecules* **2009**, *42*, 2806−2816.
(46) Ballauff, M.; Likos, C. N. *Angew. Chem., Int. Ed.* **2004**, *43*, 2998−3020.
(47) Götze, I.; Harreis, H.; Likos, C. *J. Chem. Phys.* **2004**, *120*, 7761−7771.
(48) Huißmann, S.; Likos, C. N.; Blaak, R. *Soft Matter* **2011**, *7*, 8419−8427.
(49) Pierleoni, C.; Addison, C.; Hansen, J.-P.; Krakoviack, V. *Phys. Rev. Lett.* **2006**, *96*, 128302.
(50) Pierleoni, C.; Capone, B.; Hansen, J.-P. *J. Chem. Phys.* **2007**, *127*, 171102.
(51) Capone, B.; Pierleoni, C.; Hansen, J.-P.; Krakoviack, V. *J. Phys. Chem. B* **2009**, *113*, 3629−3638.
(52) Bernabei, M.; Bacova, P.; Moreno, A. J.; Narros, A.; Likos, C. N. *Soft Matter* **2013**, *9*, 1287−1300.
(53) Heinemann, T.; Palczynski, K.; Dzubiella, J.; Klapp, S. H. *J. Chem. Phys.* **2014**, *141*, 214110.
(54) Mladek, B. M.; Gottwald, D.; Kahl, G.; Neumann, M.; Likos, C. N. *Phys. Rev. Lett.* **2006**, *96*, 045701.
(55) Lenz, D. A.; Blaak, R.; Likos, C. N.; Mladek, B. M. *Phys. Rev. Lett.* **2012**, *109*, 228301.
(56) Sciortino, F.; Zaccarelli, E. *Nature* **2013**, *493*, 30−31.
(57) Coslovich, D.; Bernabei, M.; Moreno, A. J. *J. Chem. Phys.* **2012**, *137*, 184904.
(58) Slimani, M. Z.; Bacova, P.; Bernabei, M.; Narros, A.; Likos, C. N.; Moreno, A. J. *ACS Macro Lett.* **2014**, *3*, 611−616.
(59) Georgiou, I. A.; Ziherl, P.; Kahl, G. Antinematic local order in dendrimer liquids. *Europhys. Lett.* **2014**, *106*, 44004.
(60) Kremer, K.; Grest, G. S. *J. Chem. Phys.* **1990**, *92*, 5057−5086.
(61) Rubinstein, M.; Colby, R. *Polymer Physics*; Oxford University Press: Oxford, 2003.
(62) Plimpton, S. *J. Comput. Phys.* **1995**, *117*, 1−19.
(63) Allen, M. P.; Tildesley, D. J. *Computer Simulation of Liquids*; Oxford University Press: Oxford, 1989.
(64) Ferrenberg, A. M.; Swendsen, R. H. *Phys. Rev. Lett.* **1989**, *63*, 1195.
(65) Frenkel, D.; Smit, B. *Understanding Molecular Simulation: from Algorithms to Applications*; Academic Press: Waltham, MA, 2001.
(66) Axler, S.; Bourdon, P.; Ramey, W. *Harmonic Function Theory*; Springer: Berlin, 2001; Vol. *137*.

DOI: 10.1021/acs.macromol.5b00603
Macromolecules 2015, 48, 4983−4997